Baghdad Science Journal

Volume 22 | Issue 4 Article 6

4-22-2025

Synthesis and Identification of Two Dyes Derived from p-amino phenol and Study of their Effectiveness as Corrosion Inhibitors: Experimental and Theoretical Analysis

Aseel F. Abdullah
Department of Chemistry, College of Science, University of Wasit, Kut, Iraq, aseelfarhan@uowasit.edu.iq

Sura H. Kathim
Department of Chemistry, College of Science, University of Wasit, Kut, Iraq, skathim@uowasit.edu.iq

Athra G. Sager
Department of Chemistry, College of Science, University of Wasit, Kut, Iraq, asaker@uowasit.edu.iq

Jawad Kadhim Abaies
Department of Chemistry, College of Science, University of Wasit, Kut, Iraq, jabaies@uowasit.edu.iq

How to Cite this Article

Abdullah, Aseel F.; Kathim, Sura H.; Sager, Athra G.; and Abaies, Jawad Kadhim (2025) "Synthesis and Identification of Two Dyes Derived from p-amino phenol and Study of their Effectiveness as Corrosion Inhibitors: Experimental and Theoretical Analysis," *Baghdad Science Journal*: Vol. 22: Iss. 4, Article 6.
DOI: https://doi.org/10.21123/bsj.2024.9948

BAGHDAD SCIENCE JOURNAL 2025;22(4):1131–1142

Scan the QR to view the full-text article on the journal website

RESEARCH ARTICLE

Synthesis and Identification of Two Dyes Derived from p-amino phenol and Study of their Effectiveness as Corrosion Inhibitors: Experimental and Theoretical Analysis

Aseel F. Abdullah, Sura H. Kathim, Athra G. Sager *, Jawad Kadhim Abaies

Department of Chemistry, College of Science, University of Wasit, Kut, Iraq

ABSTRACT

In this research, two dyes of p-amino phenol were synthesized by reacting the diazonium salt of p-amino phenol with aromatic compounds, including 1-naphthol and p-amino phenol. The new dyes (a and b) were identified by FT-IR, 1H-NMR, and measurements of some physical properties. The inhibitory activity of the prepared azo compounds against corrosion of carbon steel type C45 in HCl (0.1 M) medium was investigated experimentally by electrochemical measurements. The quantum mechanical method was used to calculate the geometrical structure and physical properties using the Gaussian 09 W program and the density functional theory (DFT) of B3LYP at the 6-311+G (2d, 2p) level. The DFT was utilized for the calculation of inhibition efficiency parameters for dyes that were at equilibrium geometry in vacuum media. The resulting theoretical data revealed that the optimum corrosion inhibitor was compound a.

Keywords: Azo, Corrosion inhibitor, Density functional theory, Electro chemistry, Mullikan charges

Introduction

Nowadays, compound dyes make up the major group of organic dyes in use. They are highly important materials that are used as coloring agents in the textile, paper, food, and cosmetics industries. In recent years, azo-dyes applications have contributed to the development of various technologies such as liquid crystals, organic photoconductors, and non-linear optics.[1–3] Through providing a strongly chromophoric label, azo-dyes served as important analytical tools in colorimetric, spectrophotometric, and spectrofluorimetric methods. This property is important to determine the concentration. Also, azo-dyes are important analytical compounds as they are utilized as pH and complexometric indicators and pre-concentration reagents. In terms of pharmacological, azo-dyes compounds were demonstrated that they have several bioactivities such as antibacterial, antifungal, pesticidal, antiviral, and anti-inflammatory activities.[4–6]

One of the problems that metals face is corrosion. High costs are spent annually to maintain or protect materials from corrosion. Discovering or emerging approaches to inhibit corrosion is a challenging task for scientists interested in this feild.[7] Mild steel amongst the rest of the minerals, has drawn a lot of attention as it is utilized in different fields of the mineral industry, especially in construction. The reason behind that is the fascinating property of mild steel and its relatively low-cost industry. This important material is an iron alloy. In acidic media, mild steel easily corrodes, which is considered the main drawback of this important metal. Various industrial processes including acid pickling, acid cleaning, acid descaling, and oil-wet cleaning as well as chemical laboratories considerably depend on the use of acidic solutions.[8,9] Protection or inhibiting metal

Received 13 October 2023; revised 27 January 2024; accepted 29 January 2024.
Available online 22 April 2025

* Corresponding author.
E-mail addresses: aseelfarhan@uowasit.edu.iq (A. F. Abdullah), skathim@uowasit.edu.iq (S. H. Kathim), asaker@uowasit.edu.iq (A. G. Sager), jabaies@uowasit.edu.iq (J. K. Abaies).

https://doi.org/10.21123/bsj.2024.9948

Table 1. Chemical composition of carbon steel C45.

metal	C%	Si%	Mn%	S%	P%	Cu%	Ni%	Cr%	Fe%
Carbon Steel 45	0.36–0.42	0.15–0.30	1.00–1.40	0.05	0.05	0.50	0.20	0.20	96.88 −97.49

corrosion can be attained by different methods. The main practical one is through the use of substances called inhibitors, particularly in acidic media.[10] Economic costs, availability, inhibition efficiency and pollution are the conditions that govern the choice of inhibitors. Therefore, organic materials with N, O and/or S atoms are considered the best inhibitors for mild steel corrosion in acidic media.[11,12] Adsorption of the inhibitor by the metallic surface results in the formation of an adsorbed inhibitor layer, and subsequently the occurrence of the inhibition process. The chemical features and the structures of this adsorbed layer largely effect on the inhibitors' efficacy at specific experimental circumstances.[13,14]

The present study aims to prepare new two azo-dyes of p-amino phenol and investigate their application as corrosion inhibitors via using the corrosion cell and three electrodes. the density functional theory (DFT) uses theoretical Analysis to describe the structural nature of dyes through a basis set of (B3LYP) with a 6-311+G (p, d) The theoretical corrosion inhibition parameters such as the energy of the highest occupied molecular orbital and energy of the lowest unoccupied molecular orbital, energy gap electronegativity (χ), electron affinity, global hardness, softness, ionization energy, global electrophilicity, were used for investigating and clarifying the inhibition efficiency of dyes.

Materials and methods

All chemicals were acquired from Merck, HIMIEDIA and BDH companies and they were used without any purification. *Gallenkamp*, an electro-thermal melting point apparatus was utilized to measure the melting points of compounds a and b. FI-IR spectra were recorded using 8400s-Fourier transitions, Infrared-Spectrometer-Shimadzu, Japan, the disc of KBr in the range of (4000 − 400) cm^{-1}. ^{1}H-NMR spectra of the compounds (a and b) were recorded using Bruker, Ultra-shield (500 MHz) NMR spectrometer at the University of Tehran, Iran. A corrosion cell made of Pyrex with (250 ml) capacity Consists of two vessels University of Baghdad, Iraq.

Preparation of azo dyes

Preparation of diazonium salt

p-amino phenol (0.54 g, 5 mmol) was dissolved in a mixture of (2 mL) of concentrated HCl and (5 mL) distilled water. The obtained solution was then cooled sing the ice bath at 0–5 ˚C before a solution of sodium nitroz ($NaNO_2$) (0.34 g, 5 mmol) in water (5 mL) was added drop by drop. The produced mixture was stirred for (10 min) and kept temperature at 4 ˚C. The resulting diazonium salt has been retained from the interaction for the next step (coupling reaction).[14]

General procedure for the coupling a or b compounds with phenols

α-naphthol (5 mmol) was added to 10% NaOH solution (6 ml) and cooled to 0–5 ˚C. The mixture was added drop by drop to the solution of diazonium chloride defined above with stirring. The produced mixture was left stirring for extra 1 h at 0–5 ˚C.[15] The formed colored compound was collected, washed with cooled water before it was dried at 70 ˚C. This step is repeated with compound 4-amino phenol. Table 1 displays the physical properties and spectroscopic measurements data of compounds (a and b).

The measurement of the corrosion

To set up the regulator voltage, a host computer and a thermostat were used. Magnetic stirrer, (EmStat 4s, Palm Sens, Holland) potential, and a galvanostat were also utilized. The corrosion is measured by a Pyrex cell consists of internal and external vessels. Size of the cell size was 250 ml, and it consists of three electrodes. The working electrode was the carbon steel, which utilized to measure the potential depending on a reference electrode.

The auxiliary electrode is made of platinum (10 cm), whereas the reference electrode is saturated calomel (Hg/Hg_2Cl_2 sat. KCl). To create and establish a steady-state open circuit potential (Eocp), the working electrode was immersed in a test solution for 15 minutes. Then, in a potential range of ±200 mV, the electrochemical measurements were performed. The tests of compounds (a and b) were carried out at 298 K using a cooling-heating circulating water bath. Fig. 1 shows the corrosion cell and the three electrodes. Proper dimensions of Carbon steel coupons were prepared and utilized for the standard proceedings of the corrosion evaluations. 0.1 M HCl aqueous solution was prepared as an artificial attack medium. The implemented measurements occurred according to the common corrosion procedures of steel specimens after a recorded period of immersion in an

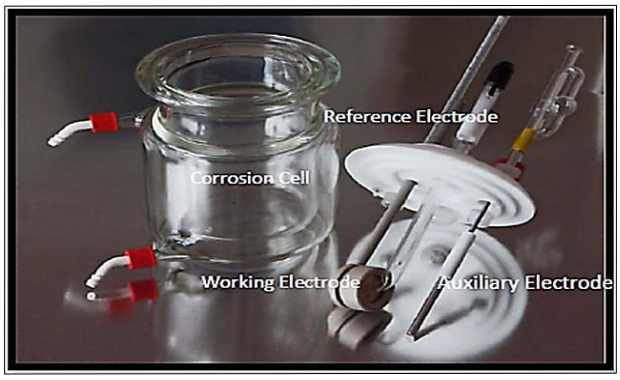

Fig. 1. Set up the corrosion cell and three electrodes.

environment under the influence of dye inhibitors at definite concentrations (25 and 50 ppm). Table 1 shows the chemical composition of carbon steel C45.

Results and discussion

The reaction of the organic compounds, a diazonium salt and a binding factor produced an azo dye. A diazonium salt (as an electrophile) was subjected to a coupling reaction with an electron-rich compound including α–naphthol and 4-aminophenol. Diazotization and coupling procedures were employed to synthesize azo dyes derived from 4-aminophenol.[14–16] Scheme 1 illustrates the synthesis of azo derivatives a and b.

The FT-IR spectra of 4-aminophenol, Fig. 2 shows two characteristic absorption bands at 3340 cm^{-1} and 3278 cm^{-1} which are attributed to υNH_2 and υOH groups respectively, 3005–3178 cm^{-1} of υ C–H aromatic and 1612 cm^{-1} of υC=C aromatic.[17] FT-IR measurements data of azo deravatives (a and b) are exhibited in Table 2. FT-IR data of compound [a] are displayed in Fig. 3. It is clearly can be seen the appearance of υ OH at (3367) cm^{-1} and υ(N=N) stretching bands at (1454) cm^{-1}.[18] Fig. 4 showed FT-IR bands of compound [b]. This figure displayed the presence of the asymmetric and symmetric stretching bands of $\upsilon(NH_2)$ absorption at 3425 cm^{-1} asym.; 3344 cm^{-1} sym Fig. 3 also exhibited the existence of the υ(N=N) stretching at 1454 cm^{-1}. ^{1}H-NMR spectrum of compound (a) is shown in Fig. 5. The spectrum exhibited the following characteristic signals δ(ppm): 6.86–8.24(m, 7H, Ar-H);10.13(s, 1H, OH). ^{1}H-NMR

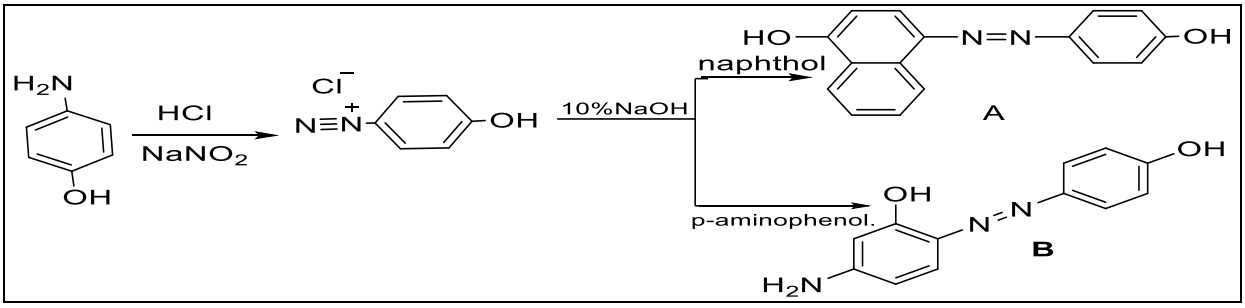

Scheme 1. Preparation route of the compounds a and b.

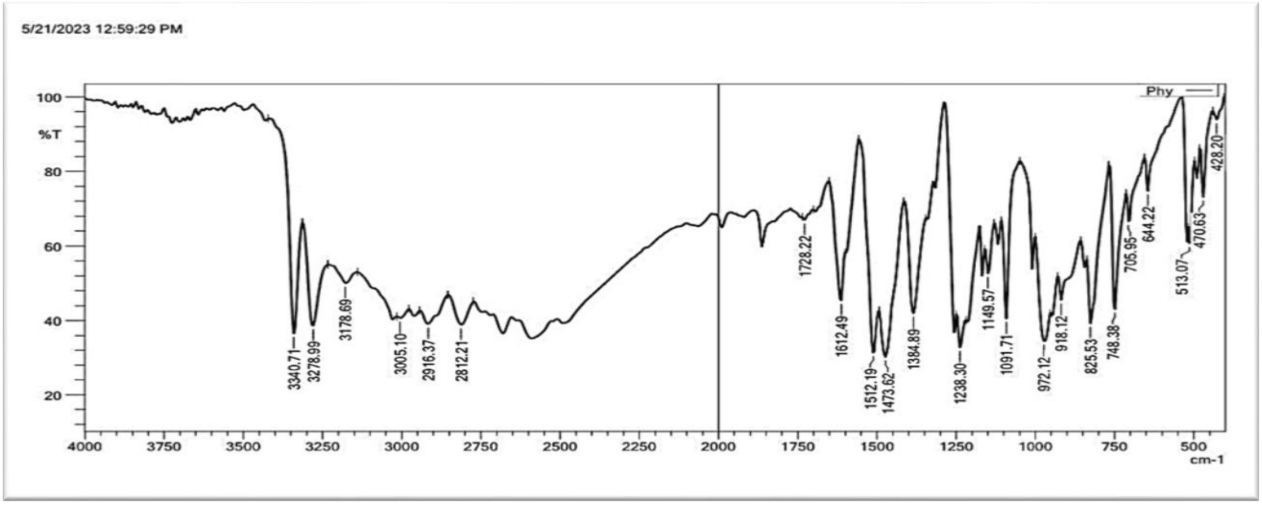

Fig. 2. FT-IR spectrum of 4-aminophenol.

Table 2. Physical properties and FT-IR spectral data of azo compounds a and b.

No.	Physical properties					FTIR /Major Absorption (cm^{-1})				
	M.P	MWt(g/mol)	Molecular structure	color	Yield %	$\upsilon(NH_2)$	υ(OH)	υ(C–H) Ar	υ(C=C) Ar.	υ(N=N)
a	100–102	264.28	$C_{16}H_{22}N_2O_2$	Dark Red	65	—	3367	3051	1597	1454
b	107–105	229.22	$C_{12}H_{11}N_3O_2$	Orange	74	3425	3344	3024	1590	1454

Table 3. ^{1}H-NMR spectral data of compounds a and b.

No.	Compound structure	^{1}H-NMR spectral data ($^{\delta}$ppm)
a	(E)-2-((4-hydroxyphenyl) diazenyl) naphthalen-1-ol	6.86–8.24 (m, 10H, Ar-H); 10.13 (s, 1H, OH, Phenol)
b	(E)-4-amino-2-((4-hydroxyphenyl) diazenyl) phenol	5.11(s, 2H.NH_2);6.20–8.15 (m, 7H, Ar-H);10.03(s, 1H, OH, Phenol)

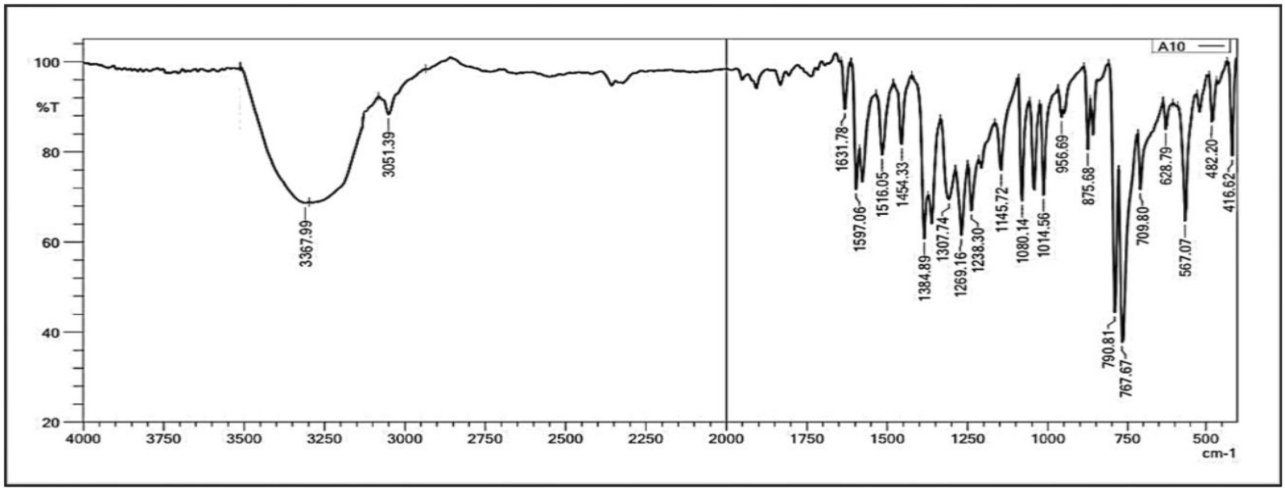

Fig. 3. FT-IR spectrum of compound a.

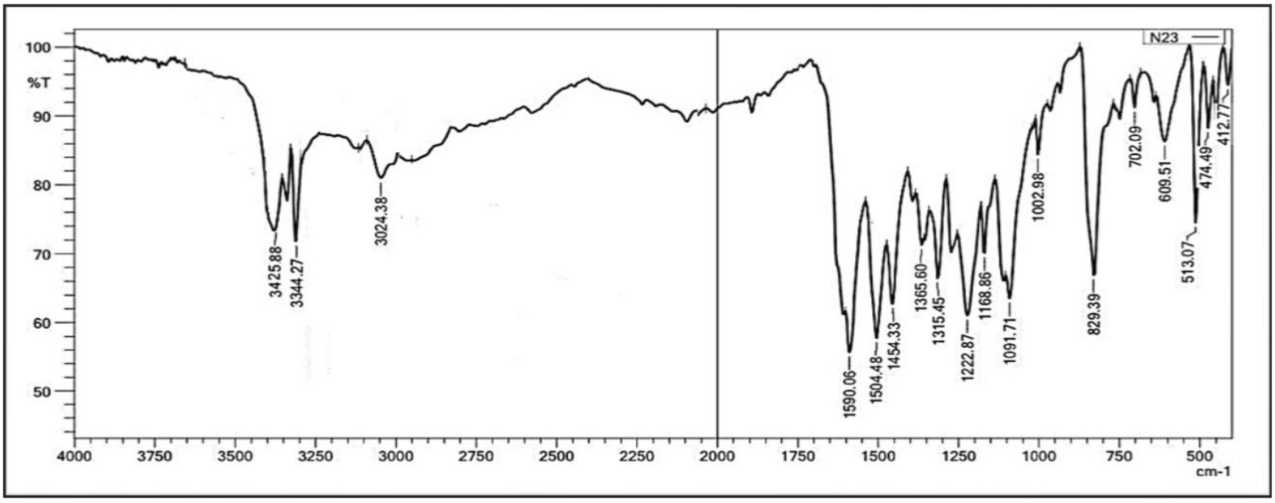

Fig. 4. FT-IR spectrum of compound b.

spectrum of compound (b) is displayed in Fig. 6. This spectrum exhibited the following characteristic signals δ(ppm): 5.11(s, 2H, NH_2);. 6.34–8.27(m, 10H, Ar-H); 10.03(s, 1H, OH). ^{1}H -NMR data of compounds (a and b) are shown Table 3.

The quantum chemical calculations of the compounds a and b

The density functional theory (DFT) was used to describe the structural nature of dyes through basis

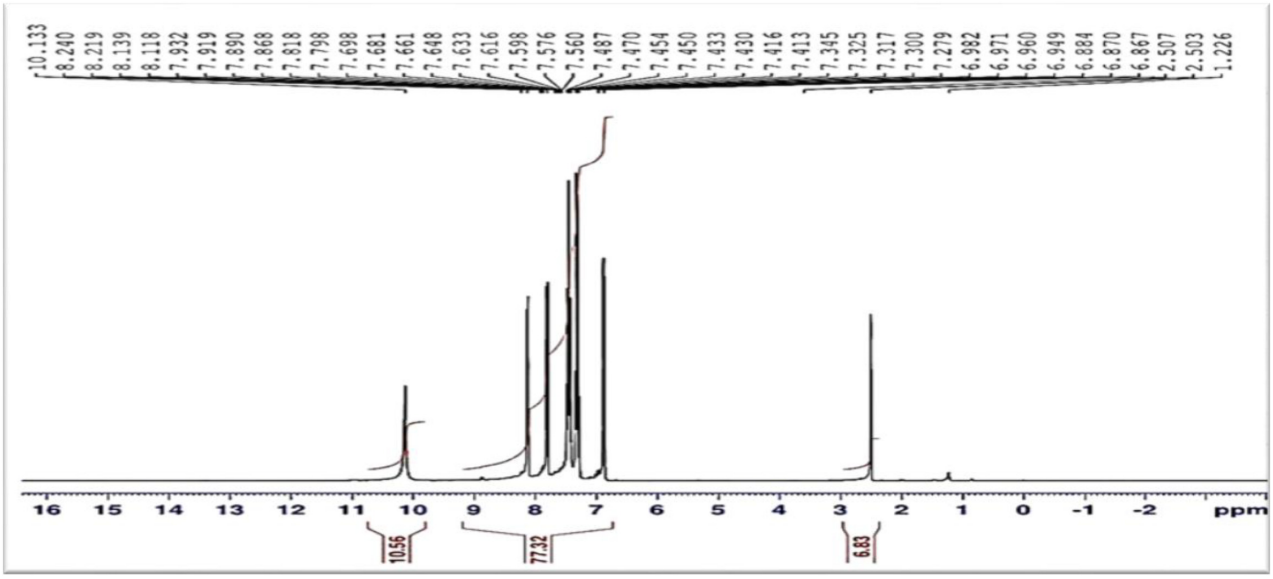

Fig. 5. ^{1}H-NMR spectrum of compound a.

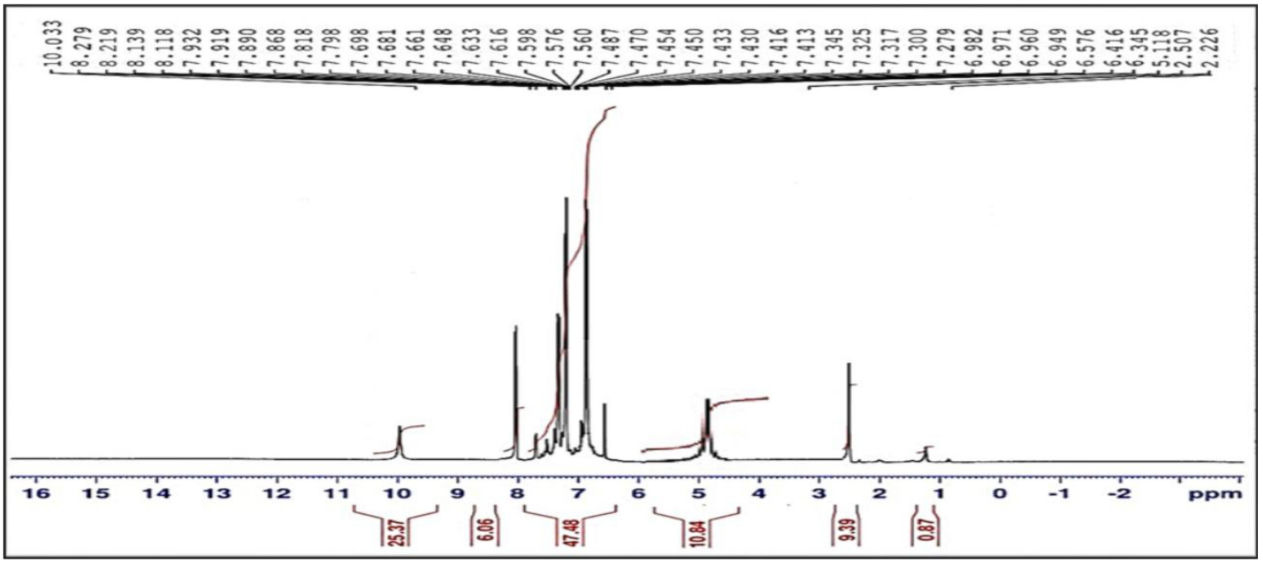

Fig. 6. ^{1}H-NMR spectrum for compound b.

set of (B3LYP) with a 6-311^{+}G (p, d). [19,20] The theoretical corrosion inhibition parameters such as "energy of the highest occupied molecular orbital (EHOMO) and energy of the lowest unoccupied molecular orbital (ELUMO), energy gap (ΔE) between EHOMO and ELUMO, dipole moment (μ), electronegativity (χ), electron affinity (A), global hardness (η), softness (σ), ionization energy (IE), global electrophilicity (ω), the fraction of electrons transferred (ΔN) and the total energy (E_{tot})" [21] were used for investigation and clarifying the inhibition efficiency of compounds. The compounds (a and b) were designed using ChemDraw. ChemDraw program was used to draw the structures compounds. The program (Gaussian 09W) was employed to compute the molecular geometry. [22] The corresponding geometry was calculated at a vacuum phase. Fig. 7 shows the atoms numbering of compounds a and b. The bond angles, bond distances, and dihedral angles were computed and investigated as structural parameters of compounds a and b as shown in Table 4.

Length bond was observed of compound (a) for C8-C9 (1.39164A °). The shortest bond length was observed for O11H27 (0.97133A °). The bond angles were locating between (107.462A °) for N20N19C14 and (120.02678A °) for N19C14C15. The dihedral

Table 4. The bond length, distances, and dihedral angles for compounds a and b in media of vacuum as calculated by using DFT method.

Description Bond length	Bond length (Å)	Description angle (deg)	Angle (deg)	Description Dihedral Angle (deg)	Dihedral angle (deg)
			Compound a		
$N_{20}N_{19}$	1,24861	$N_{20}N_{19}C_{14}$	107.46128	$C_{14}N_{20}N_{19}C_{27}$	179.94297
$O_{11}C_{10}$	1.35525	$O_{11}C_{10}C_{9}$	119.61113	$O_{11}C_{10}C_{5}C_{4}$	179.97257
$O_{18}C_{17}$	1.35474	$O_{18}C_{17}C_{16}$	119.99817	$O_{18}C_{17}C_{12}C_{13}$	−179.98368
$N_{20}C_{7}$	1.26032	$N_{20}C_{7}C_{4}$	119.63226	$N_{20}C_{7}C_{4}C_{5}$	179.97646
$N_{19}C_{14}$	1.25991	$N_{19}C_{14}C_{15}$	120.02678	$C_{14}N_{19}N_{20}C_{7}$	179.94297
$O_{11}H_{27}$	0.97133	$H_{27}O_{11}C_{10}$	107.98579	$H_{27}O_{11}C_{10}C_{9}$	179.97226
$O_{18}H_{32}$	0.97168	$H_{32}O_{18}C_{17}$	108.03875	$H_{32}O_{18}C_{17}C_{16}$	−179.93969
$C_{8}C_{9}$	1.39164	$C_{8}C_{9}C_{10}$	119.97430	$C_{8}C_{9}C_{10}O_{11}$	−179.97312
$C_{15}H_{30}$	1.09966	$H_{30}C_{15}C_{14}$	120.02140	$H_{30}C_{15}C_{14}C_{13}$	−179.96757
			Compound b		
$N_{28}C_{27}$	1.26659	$N_{28}C_{27}C_{26}$	119.99593	$N_{28}C_{27}C_{26}C_{22}$	−179.98725
C_{22} O_{21}	1.35476	$O_{21}C_{22}C_{26}$	120.04644	$O_{21}C_{22}C_{26}C_{27}$	−170.98385
$N_{12}N_{13}$	1.24796	$N_{12}N_{13}C_{18}$	107.50440	$C_{18}N_{13}N_{12}C_{23}$	−179.98777
$N_{12}C_{23}$	1.26072	$N_{12}N_{13}C_{23}$	107.51378	$N_{12}C_{23}C_{24}C_{25}$	179.98281
$O_{14}C_{15}$	1.35450	$O_{14}C_{15}C_{16}$	120.02373	$O_{14}C_{15}C_{28}C_{19}$	179.98921
$N_{28}H_{10}$	1.05094	$C_{27}N_{28}H_{10}$	119.95978	$H_{10}N_{28}C_{27}C_{25}$	−179.94175
$N_{28}H_{11}$	1.04980	$C_{27}N_{28}H_{11}$	120.04447	$H_{11}N_{28}C_{27}C_{26}$	−179.99596
$C_{26}C_{22}$	1.39528	$C_{26}C_{22}C_{23}$	119.94271	$C_{26}C_{22}O_{21}H_{3}$	−179.97975

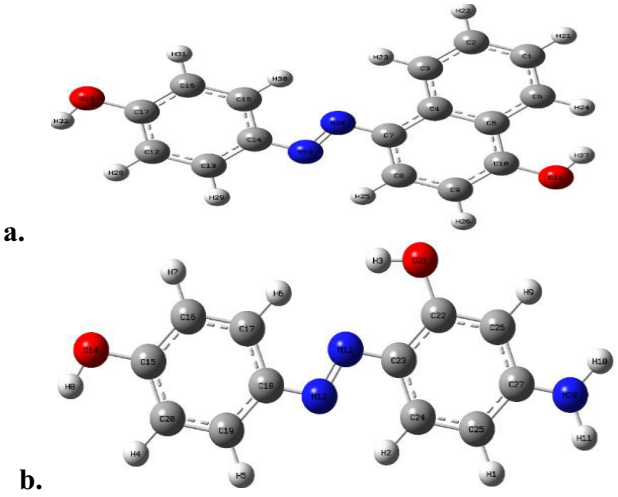

Fig. 7. The numbering of atoms of compounds a and b.

angles values (trans and cis) demonstrated that the compound was not planar and dihedral angles are not 0.0 degrees. While, Table 4 shows the longest bond length that was noticed, which belongs to compound (b) for C22-C26(1.39528A °). The shortest bond length was noticed for N28-H11 (1.0498A °). The bond angles were locating between (107.5044A °) for O21C22C26 and (120.046A °) for O21C22C26. The dihedral angles values (trans and cis) demonstrated that the compound was not planar.

Global reactivity of molecular

In order to predict the adsorption centers of compounds [a and b], the frontier orbital theory was utilized. The centers of adsorption in compounds a and b will have a significant role in inhibition the reaction of metal surface/molecule (a and b). [23]

Tables 5 to 7 show the calculated quantum chemical parameters. The calculation of parameters were carried out using the following vital equations:

$$IP = -EHOMO \tag{1}$$

$$EA = -ELUMO \tag{2}$$

$$H = \frac{IE - EA}{2} \tag{3}$$

$$X = \frac{IE + EA}{2} \tag{4}$$

$$S = \frac{1}{\eta} \tag{5}$$

$$\omega = \frac{-X^2}{2\eta} = \frac{\mu^2}{2\eta} \tag{6}$$

Where: IP = Ionization potential; EA = Electron affinity; H = Hardness;

χ = Electro negativity, softness = S; the Global electrophilicity index = ω; the electrons transferred = Δ N.

Table 5 shows the geometry structure of compounds a and b in a vacuum. The geometry structure consists density distributions of HOMO and LUMO. The location of HOMO is mostly on the diazine moiety. Accordingly, the location of the favorite actives sites for the attack by electrophile are in the region that surround N atoms and O atoms. While,

Table 5. Frontier Molecular Orbital density distributions of compounds a and b.

NO.	HOMO D3	LOMO D3
a	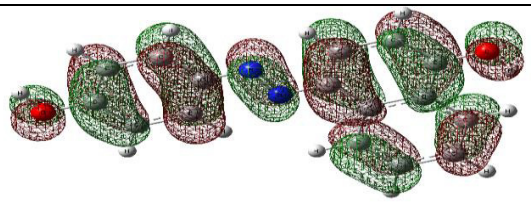	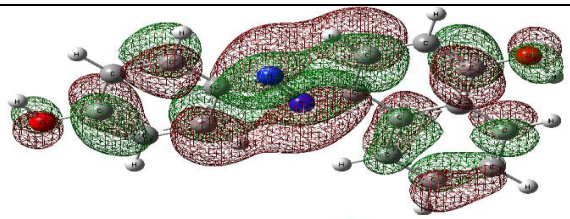
b	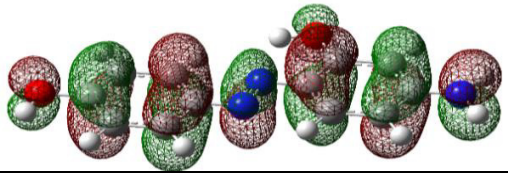	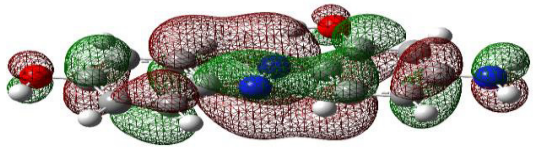

Table 6. The some physical properties of the inhibitor molecules a and b at the equilibrium geometry by using DFT method.

No.	Molecular formula	EHOMO(eV)	ELOMO(eV)	ΔE(eV)	μ(Debye)
a	$C_{16}H_{22}N_2O_2$	−5.1539528	−2.743242	2.41071	0.187156
b	$C_{12}H_{11}N_3O_2$	−4.8883637	−2.306489	2.58187	4.245720

Table 7. Quantum chemical parameters for inhibitor molecules [a and b] by using DFT method.

No.	IE (eV)	EA (eV)	η (eV)	μ (eV)	X (eV)	S (eV)	ω (eV)	Δ N (e)	N_{max}	CP
a	5.15395	2.74324	1.205	−3.94	3.9486	0.82963	6.46756	1.26577	3.27588	−3.9486
b	4.88836	2.30649	1.290	−3.59	3.59743	0.77463	5.01243	1.31787	2.78668	−3.5974

LUMO electronic density was distributed around the aromatic ring and surround diazine moiety, which implies the majority of planar region is in the compound molecules.

The global chemical reactivity descriptor ($\mu = -\chi$) describes a chemical potential. The chemical potential (μ) measures the escaping of an electron and describes the molecular electronegativity. If (μ) was more negative, the molecular would lose an electron easier. In a comparison with compound a, compound b is less stable and more reactive. Nevertheless, electronegativity of compound a is bigger than that of compound b as illustrated in Table 7. Hardness (η) and softness (S) will useful concepts in understanding the behavior of atoms. The values of these parameters were theoretically calculated. The calculation data revealed that the compound b possesses the biggest hardness value (η = 1.29 eV). This implies that the hardest molecule is b. The molecule possesses the biggest softness = 0.82963, which means that it is the softest molecule. The value electrophilicity (ω) gives knowledge about the stabilization energy become the system becomes rich with electrons that moved from ambient. On the other hand, the molecule b with the slightest values of ω = 5.01243, so the compound (b) is good nucleophile. While, the molecule a is a good electrophile as it has the highest value of (ω = 6.46756).

Local reactivity descriptors

Calculating Fukui functions will help researchers to understand the active site of molecules. Chemical reaction depends on a variation in the electrons number, which requires a minimum one electron being added or subtracted in the frontier orbitals.

Fukui functions $f^{+}_{(r)}$, $f^{-}_{(r)}$ and $f^{0}_{(r)}$ are calculated by the following equations:

$$\text{“}f+ = [q(N+1) - q(N)]. \text{ for nucleophilic attack} \quad (7)$$

$$f^{-} = [q(N) - q(N-1)] \text{ for electrophilic attack} \quad (8)$$

$$f^{0} = [q(N+1) - q(N-1)]2. \text{ for radical attack}''. \quad (9)$$

Where : q(N) = the charge located on the atom for neutral molecule; q(N + 1) = anionic specie, and (N − 1) = cationic specie.[23,24]

The values of descriptors chemical were calculated at level of B3LYP/6-31G (d, p) by Mulliken charges on molecules atoms. For compound a, the greatest preferred susceptible spot for a nucleophilic attack is placed on 18O. Nonetheless, the greatest reactive position for electrophilic attack is placed on19N. The most preferred reactive spot for a free radical attack is on 19N. Moreover, 14O is the greatest susceptible

Table 8. Values of the Fukui function of the molecules a and b.

compound	a			b			
Atom	*f+*	*f–*	*f0*	Atom	*f+*	*f–*	*f0*
1c	−0.03179	−0.0311	−0.03145	1H	0.046628	0.046077	0.046353
2C	0.033693	0.048078	0.040886	2H	0.02935	0.023057	0.026204
3c	0.025342	0.002745	0.014044	3H	0.010092	0.00471	0.007401
4C	−0.00055	0.02515	0.012303	4H	0.044667	0.041944	0.043306
5C	0.0073	−0.01149	−0.0021	5H	0.040118	0.036555	0.038337
6C	0.042677	0.040163	0.04142	6H	0.029109	0.017074	0.023092
7C	0.042619	−0.00319	0.019714	7H	0.04166	0.041516	0.041588
8C	−0.00025	0.05186	0.025805	8H	0.023755	0.021577	0.022666
9C	0.016095	−0.00459	0.005752	9H	0.044667	0.042289	0.043478
10C	0.056801	0.059623	0.058212	10H	0.041525	0.036862	0.039194
11O	0.071532	0.054533	0.063033	H11	0.040056	0.033689	0.036873
12C	0.033864	0.03032	0.032092	12N	0.01719	0.073392	0.045291
13C	0.04155	0.042922	0.042236	13N	0.05246	0.115838	0.084149
14C	−0.02119	−0.05335	−0.03727	14O	0.069577	0.042217	0.055897
15C	0.038535	0.077687	0.058111	15C	0.051462	0.061068	0.056265
16C	0.021152	−0.00517	0.007993	16C	0.028642	−0.01169	0.008476
17C	0.051751	0.066749	0.05925	17C	0.021473	0.063209	0.042341
18O	0.064727	0.042648	0.053688	18C	−0.00898	−0.02794	−0.01846
19N	0.038896	0.108636	0.073766	19C	0.046861	0.053268	0.050065
20N	0.023712	0.051386	0.037549	20C	0.041643	0.045354	0.043499
21H	0.038692	0.03693	0.037811	21O	0.052689	0.046941	0.049815
22H	0.03627	0.034544	0.035407	22C	0.046207	0.056832	0.05152
23H	0.019388	0.011125	0.015257	23C	0.046946	−0.00419	0.021379
24H	0.032347	0.031515	0.031931	24C	0.006671	0.07539	0.041031
25H	0.031725	0.022378	0.027052	25C	0.019067	−0.04012	−0.01053
26H	0.042547	0.040136	0.041342	26C	0.006753	−0.0125	−0.00287
27H	0.018797	0.015929	0.017363	27C	0.059635	0.095435	0.077535
28H	0.041627	0.039983	0.040805	28N	0.050082	0.02214	0.036111
29H	0.036923	0.035455	0.036189				
30H	0.022104	0.01725	0.019677				
31H	0.037277	0.038064	0.037671				
32H	0.022262	0.020878	0.02157				

spot to nucleophilic attack for compound b. Whereas, the greatest susceptible spot for both electrophilic and free radical attacks is on 13N Table 8.

Corrosion study

Potentiodynamic polarization curves and corrosion kinetic

Extraction of polarization curves for carbon steel corrosion of the synthesized inhibitors (a and b) was achieved in HCl solution. The extraction of polarization curves was carried out at (25, 50 ppm) concentrations of (a and b) inhibitors and the ambient temperature was 298 Kelvin in the existence and absence of the inhibitors as displayed in Fig. 8. This figure also shows polarization curves for the molecules (a and b) and the blank (HCl solution). The electrochemical corrosion parameters such as corrosion potential (E_{corr}), and corrosion current density (I_{corr}) attained by cathodic and anodic areas of the Tafel lines were described in Table 9.

IE% and Θ were calculated by the following:[25]

$$\%IE = (I_{corr(uninh)} - I_{corr(inh)}/I_{corr(uninh)}) \times 100. \quad (10)$$

$$\Theta = (I_{corr(uninh)} - I_{corr(inh)}/I_{corr(uninh)}) \quad (11)$$

Where: $I_{corr(inh)}$ = current densities of inhibited corrosion, $I_{corr\ (uninh)}$ = uninhibited current densities.

Table 9 illustrates that at a temperature of 298 K, the value (IE%) of the molecule (a) is bigger than that of the compound (b). This demonstrates the physisorption inhibition occurrence. These results disclose that at 25 and 50 ppm concentrations of molecules a and b, the Icorr value is reduced, which indicates that these compounds are good inhibitors of corrosion. Moreover, besides increasing the concentration of inhibitors, a minor change in E_{corr} to negative values is caused by molecules a and b, resulting in an improvement in inhibition efficiency. Also, it was found that the highest inhibition efficacy was up to 91%, belonging to compound a with a

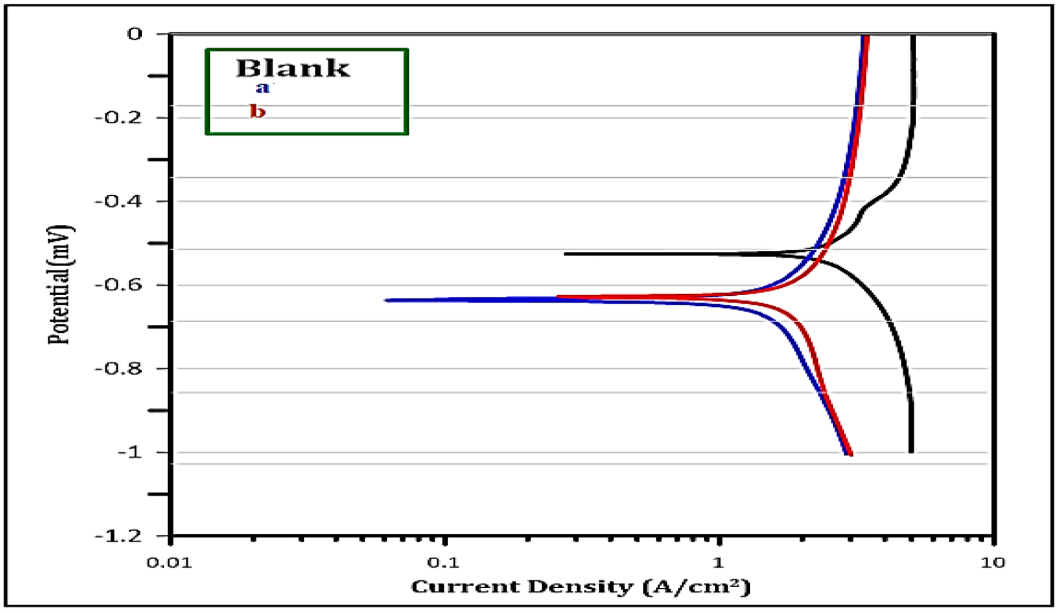

Fig. 8. Polarization curves for compound a and b (25 ppm) at 298 K.

Table 9. Corrosion parameters for blank and compounds a and b in (0.1 M) HCl solutions.

Comp	C (ppm)	E corr. vs. SCE (mV)	I corr. (mA cm^{-2})	I corr./r	Resis.	Anodic b_a (mV Dec^{-1})	Cathodic $-b_c$ (mV Dec^{-1})	Corr. rate,	IE%	Θ
Blank		−0.527	163.5	3.269E-4	143.2	0.126	0.094	1.605	—	—
a	50	−0.630	15.36	3.073 E-5	2957	0.167	0.279	0.151	91	0.91
	25	−0.637	16.33	266.E-5	2109	0.127	0.213	0.160	90	0.90
b	25	−0.634	28.43	5.685 E-5	1690	0.189	0.276	0.279	83	0.83
	50	−0.638	23.99	5.798E-5	1880	0.175	0.255	−0.618	85	0.85

concentration of 50 ppm and at a temperature of 298 K. This is attributed to the existence of groups with high electronic density including phenyl rings, hydroxyl groups, N2 atoms, and Pi bonds, which participate in the generation of coordination links with the metal surface. Accordingly, a preservative layer will be formed on the metal surface in acidic medium, and subsequently prevents carbon steel corrosion.

A study of the temperature effect on efficiency of inhibition was not achieved and it will be applied in a later study. It was suggested that the temperature might increase the mobility of the inhibitor molecules, resulting in a reduction in the contact between the inhibitor molecules and the carbon steel surface.

The inhibitor molecules motion increases as temperature increases.[26]

Conclusion

The values of the theoretical chemical parameters suggest that compound (a) has a greater tendency to interact with the metal surface in a vacuum, and it is a good inhibitor. The results of density functional theory (DFT) were used to describe the structural nature of dyes through a basis set of (B3LYP) with 6-311+G (p, d) calculations on p-amino phenol derivatives that have been presented in a vacuum. The HOMO, LUMO, and charges on atoms predict a similar center (N=N) that would prefer to be attacked by nucleophilic or electrophilic species. The results of DFT/B3LYP were closer to the experimental data. Experimentally, it was observed that the corrosion of carbon steel C45 in the corrosive medium with compound (a) inhibitor was decreased. Also, compound (a) inhibition efficiency in the HCl solution was (91%).

Acknowledgment

The authors are thankful to the University of Wasit for supporting this research, and the University of Basra for the help in providing the analysis techniques for our samples.

Author's declaration

– Conflicts of Interest: None.

- We hereby confirm that all the Figures and Tables in the manuscript are ours. Furthermore, any Figures and images, that are not ours, have been included with the necessary permission for re-publication, which is attached to the manuscript.
- No animal studies are present in the manuscript.
- No human studies are present in the manuscript.
- No potentially identified images or data are present in the manuscript.
- Ethical Clearance: The project was approved by the local ethical committee at University of Waist.

Author's contribution statements

A. G. S., A. F. A., S. H. K., and J. K. A. contributed to the design and implementation of the research, to the analysis of the results, and to the writing of the manuscript.

References

1. Kamoon RA, Al-Mudhafar MMJ, Omar TN-A. Synthesis. Characterization and Antimicrobial Evaluation New Azo Compounds Derived from Sulfonamides and Isatin Schiff Base, Int J Drug Delivery Tech. 2020;10(1):150–155. http://dx.doi.org/10.25258/ijddt.10.1.22.
2. Ibraheem IH, Mubder NS, Abdullah MA, Al-Neshmi H. Synthesis, characterization and bioactivity Study from azo –ligand derived frommethyl-2-amino benzoate with some metal ions. Baghdad Sci J. 2023;20(1):114–120. https://doi.org/10.21123/bsj.2022.6584.
3. Benkhaya S, M'rabet S, El Harfi A. Classifications, properties, recent synthesis and applications of azo dyes. Heliyon. 2020 Jan 31;6(1):e03271. https://doi.org/10.1016/j.heliyon.2020.e03271.
4. Mezgebe K, Mulugeta E. Synthesis and pharmacological activities of azo dye derivatives incorporating heterocyclic scaffolds: a review. RSC Adv. 2022 Sep 13;12(40):25932–25946. https://doi.org/10.1039/d2ra04934a.
5. Tahir T, Ashfaq M, Saleem M, Rafiq M, Shahzad MI, Kotwica-Mojzych K, *et al*. Pyridine Scaffolds, Phenols and Derivatives of Azo Moiety: Current Therapeutic Perspectives. Molecules. 2021 Aug 11;26(16):4872–4828. https://doi.org/10.3390/molecules26164872.
6. Al-Khuzaie MGAn, Al-Majidi SMH. Synthesis and characterization of new azo compounds linked to 1,8-naphthalimide as new fluorescent dispersed dyes for cotton fibers. AIP Conf Proc. 2020;2290:030011. https://doi.org/10.1063/5.0027354.
7. Aftan MM, Toma MA, Dalaf AH, Kaain, H. Synthesis and Characterization of New Azo Dyes Based on Thiazole and Assess the Biological and Laser Efficacy for Them and Study their Dyeing Application. Egypt J Chem. 2021;64(6):2903–2911. https://doi.org/10.21608/ejchem.2021.55296.3163.
8. Kmal RQ, Mohamed AM, Aljeboree AM, Jasim LS, Alkaim AF. Synthesis and Identification of Azo Disperse Dye Derived from 4-Aminoantipyrine and Their Applications to Determine Some Drugs. Int J Drug Delivery, 2021;11(3):1040–1044. https://doi.org/10.25258/ijddt.11.3.67.
9. Franco JH, da Silva BF, Dias EFG, de Castro AA, Ramalho TC, Zanoni MVB. Influence of auxochrome group in disperse dyes bearing azo groups as chromophore center in the biotransformation and molecular docking prediction by reductase enzyme: Implications and assessment for environmental toxicity of xenobiotics. Ecotoxicol Environ Saf. 2018 Sep 30;160:114–126. https://doi.org/10.1016/j.ecoenv.2018.04.066.
10. Zobeidi A, Neghmouche Nacer S, Atia S, Kribaa L, Kerassa A, Kamarchou A, *et al*. Corrosion Inhibition of Azo Compounds Derived from Schiff Bases on Mild Steel (XC70) in (HCl, 1 M DMSO) Medium: An Experimental and Theoretical Study. ACS Omega. 2023 Jun 5;8(24):21571–21584. https://doi.org/10.1021/acsomega.3c00741.
11. Lessa RCdS. Synthetic Organic Molecules as Metallic Corrosion Inhibitors: General Aspects and Trends. Organics. 2023;4(2):232–250. https://doi.org/10.3390/org4020019.
12. Khudhair NA, Kadhim MM, Khadom AA. Effect of Trimethoprim Drug Dose on Corrosion Behavior of Stainless Steel in Simulated Human Body Environment: Experimental and Theoretical Investigations. J Bio- Tribo-Corros. 2021;7(3):8–13. https://doi.org/10.1007/s40735-021-00559-8.
13. Fawzy A, Toghan A. Inhibition Evaluation of Chromotrope Dyes for the Corrosion of Mild Steel in an Acidic Environment: Thermodynamic and Kinetic Aspects. ACS Omega. 2021 Jan 25;6(5):4051–4061. https://doi.org/10.1021/acsomega.0c06121.
14. Mustafa SR, Al-Ani HN. Calculation of vibrational frequencies, Energetic and some other Quantum Chemical Parameters for some Flavonoids, J Phys Conf Ser. 2021(1):12018. https://doi.org/10.1088/17426596/1999/1/012018.
15. Abdulridha MQ, Al-hamdani AAS, Hussein IA. Synthesis, Characterization and Antioxidant Activity of New Azo Ligand and Some Metal Complexes of Tryptamine Derivatives. Baghdad Sci J. 2023;20:1046–1063. https://doi.org/10.21123/bsj.2023.8227.
16. Naser AW, Abdullah AFJ. Synthesis of some new N-saccharin derivatives of possible biological activity. Chem Pharm Res. 2014;6(5):872–879.
17. Mohammed HS, Al-Saadawy NH. Synthesis, Characterization and Theoretical Investigation of Innovative Charge-transfer Complexes Derived from the N-phenyl 3, 4-selenadiazo Benzophenone Imine. Baghdad Sci J. 2023;20(5):1943–1963. https://doi.org/10.21123/bsj.2023.7748.
18. Dhumad AM, Hassan QM, Fahad TA, Emshary CA, Raheem NA, Sultan HA. Synthesis, structural characterization and optical nonlinear properties of two azo-β-diketones. J. Mole. Struct. 2021;5 July(1235):130196. https://doi.org/10.1016/j.molstruc.2021.130196.
19. Kudelko A, Olesiejuk M, Luczynski M, Swiatkowski M, Sieranski T, Kruszynski R. 1,3,4-Thiadiazole-Containing Azo Dyes: Synthesis, Spectroscopic Properties and Molecular Structure. *Molecules*. 2020;25(12):2822–2839. https://doi.org/10.3390/molecules25122822.
20. Ahmed MA, Jasdeep K, Akhil S, Mahmoud AB, Dakeshwar KV, Elyor B. Electrochemical and DFT studies of Terminalia bellerica fruit extract as an eco-friendly inhibitor for the corrosion of steel. Nature. 2023;13(19367):1–22. https://doi.org/10.1038/s41598-023-45283-0.
21. Mahmoud AB, Hani ME, Ahmed B, Rabab MA, Abed El-ziz SF. Novel coumarin-buta-1,3-diene conjugated donor–acceptor systems as corrosion inhibitors for mild steel in 1.0 M HCl: Synthesis, electrochemical, computational and SRB biological resistivity. Sci Direct. 2023;148(15):128644. https://doi.org/10.1016/j.inoche.2022.110304.
22. Kubba MR, Abood KF. DFT, PM3, AM1, and MINDO/3 Quantum Mechanical Calculations for Some INHC Cs Symmetry

Schiff Bases as Corrosion Inhibitors for Mild Steel. Iraqi J Sci. 2023;56(1C):602–621. https://doi.org/10.9734/bpi/mono/978-93-91882-61-7/CH5.

23. Mahmoud AB, Hani ME, Ahmed HB, Rabab MA, Abed El-ziz SF. Novel coumarin-buta-1,3-diene conjugated donor–acceptor systems as corrosion inhibitors for mild steel in 1.0 M HCl: Synthesis, electrochemical, computational and SRB biological resistivity. Sci Direct. 2023;148(15):128644. https://doi.org/10.1016/j.inoche.2022.110304.
24. Kubba RM, Mohammed MA. Theoretical and Experimental Study of Corrosion Behavior of Carbon Steel Surface in 3.5% NaCl and 0.5 M HCl with Different Concentrations of Quinolin2-One Derivative. Baghdad Sci J. 2022;19(1):105–120. https://doi.org/10.21123/bsj.2022.19.1.0105.
25. Ahmed AH, Kuba RM, Al-Majidi SMH. Synthesis, Identification, Theoretical and Experimental Studies of Carbon Steel Corrosion Inhibition in Sea Water by Some New Diazine Derivatives linked to 5-Nitro Isatin Moiety. Iraqi J Sci. 2018;59(3B):1347–1365. https://doi.org/10.24996/ijs.2018.59.3B.2.
26. Khudhair NA, Bader AT, Ali MI, Husseini M. Synthesis, identification and experimental studies for carbon steel corrosion in hydrochloric acid solution for polyimide derivatives. AIP Conf Proc. 2020;2290(1):030014. https://doi.org/10.1063/5.0027443.

تحضير وتشخيص صبغتين مشتقتين من بارا- أمينو فينول ودراسة فعاليتهما كمثبطات للتآكل: التحليل التجريبي والنظري

اسيل فرحان عبد الله ، سرى حامد كاظم، عذراء كطامي صكر ، جواد كاظم عبيس

قسم الكيمياء ، كلية العلوم ، جامعة واسط ، الكوت ، العراق.

الخلاصة

تم في هذا البحث تحضير صبغتين من بار-امينو فينول من خلال تفاعل ملح الديزونيوم من بارا-امينو فينول مع مركبين اروماتي (1-نفثول وبارا-امينو فينول). تم تشخيص الصبغتين الجديدتين (a و b) بتقنية FTIR و^{1}HNMR مع قياس بعض الخواص الفيزيائية. تم دراسة النشاط التثبيطي تجريبياً بواسطة القياسات الكهروكيميائية لمركبات الآزو المحضرة ضد تآكل الفولاذ الكربوني نوع C45 في وسط (0.1 M, HCl). تم استخدام طريقة ميكانيكة الكم لحساب البنية الهندسية والخواص الفيزيائية بواسطة برنامج Gaussian 09 W ونظرية الكثافة الوظيفية (DFT) لدالة B3LYP بمستوى 6-311 G^{+} (2d, 2p) . تم استخدام نظرية الكثافة الوظيفية في حساب معاملات كفاءة التثبيط للصبغتين في وسط مفرغ من الهواء, وأظهرت النتائج ان المركب a الافضل بالتثبيط.

الكلمة المفتاحية: آزو، مثبط التآكل، نظرية الكثافة الوظيفية، الكيمياء الكهربائية، شحنات موليكين.